Unusual magnetic and magnetostriction behavior around the magnetic compensation temperature in Co_2TiO_4

Qing-Yuan Liu,[1] Hong-liang Wang,[2] Xin-zhi Liu,[3,*] Lei Tao,[4] Jian Liu,[4] Dong-feng Chen,[2] Kai Sun,[2] Zi-Yi Liu,[1,5] Jin-Guang Cheng,[5] Ming-Xue Huo,[4] Xian-Jie Wang,[1] and Yu Sui[1,4,†]

[1]*School of Physics, Harbin Institute of Technology, Harbin 150001, China*

[2]*Neutron Scattering Laboratory, Department of Nuclear Physics, China Institute of Atomic Energy, Beijing 102413, China*

[3]*Centre for Physical Mechanics and Biophysics, School of Physics, Sun Yat-sen University, Guangzhou 510275, China*

[4]*Laboratory for Space Environment and Physical Sciences, Harbin Institute of Technology, Harbin 150001, China*

[5]*Beijing National Laboratory for Condensed Matter Physics and Institute of Physics, Chinese Academy of Sciences, Beijing 100190, China*

(Received 6 February 2021; revised 3 May 2021; accepted 22 July 2021; published 4 August 2021)

Some intricate behaviors have been reported at magnetic compensation temperature in Co_2TiO_4 (CTO), but their origins are still unclear. In this paper, we investigate systematically the anomalous properties in CTO crystal by using direct and alternating current magnetic susceptibilities, specific heat, thermal expansion, magnetostriction, and neutron diffraction measurements. CTO exhibits a ferrimagnetic ordering transition at $T_C \approx 48$ K and a magnetic compensation behavior at $T_{comp} \approx 31$ K. Under zero field, there is no obvious anomaly in CTO around ferrimagnetic compensation temperature T_{comp}, but a minimum value of $M(T)$, a drop of $\chi'(T)$, a step of $\Delta L/L_{80\,K}$ and a sharp specific heat peak all occur at T_{comp} under the same critical magnetic field of 20 kOe. We propose a phenomenological model to explain these anomalous phenomena, in which the 180° reversal of the ferrimagnetic component at T_{comp} under $H \geqslant 20$ kOe, as well as the deflection of the oblique spin moments at B sites under magnetic field, play a key role in how to understand them.

DOI: 10.1103/PhysRevB.104.064407

I. INTRODUCTION

Spinel oxides with a general formula AB_2O_4 (A and B are usually transition metal ions) have attracted great interest due to a wide range of exciting physical properties such as multiferroic, negative thermal expansion, magnetodielectric, and magnetic shape memory effect [1–5]. In spinel oxides, the competition of exchange interactions J_{AA}, J_{BB}, and J_{AB}, which are the interactions between A-A, B-B, and A-B, give rise to various magnetic structure, such as collinear (Néel) and noncollinear (Yafet-Kittel) ferrimagnetic ordering, spiral ordering, spin glass, and spin liquid [6–11]. Furthermore, Co_2TiO_4 (CTO) was reported to be a rare example showing the unusual semi-spin-glass (SSG) behavior after ferrimagnetic ordering, in which the ferrimagnetic-ordered longitudinal component coexists with the disordered transverse component freezing into spin-glass state [12].

CTO belongs to the inverse spinel $(B)_T(AB)_OO_4$, where the subscripts T and O represent tetrahedron and octahedron, respectively, and its electronic configuration is believed to be $(Co^{2+})_T[Co^{3+}Ti^{3+}]_OO_4$ [13]. CTO was reported to exhibit a quasi-long-range ferrimagnetic ordering transition at $T_C \approx 48$ K and a magnetic compensation behavior at $T_{comp} \approx 32$ K [13–16]. According to Villain's [17] theory, nonmagnetic impurities or other forms of disorder at B sites in spinel oxides could transform the ferrimagnetic ordering into an SSG state, and the SSG magnetic structure of CTO was also confirmed using magnetic and neutron-diffraction measurements by Hubsch and Gavoille [12]. However, Nayak *et al.* [13] found that the relaxation time fitted from the alternating current (AC) susceptibility by using the Vogel-Fulcher law gives an unphysical value, indicating the lack of spin-glass state in CTO. Though the spin-glass behavior was further verified recently by AC susceptibility and critical exponents measurements, the freezing temperatures were reported to be 46.85 K by Thota *et al.* [18] and 22.39 K by Liu *et al.* [19]. Moreover, Srivastava *et al.* [20] pointed out that there are up to five peaks of AC susceptibility, suggesting more than one spin-glass transition in CTO. Thus, there is still a controversy whether the SSG state exists in CTO. More importantly, the influence of SSG on the physical properties remains undisclosed.

In fact, some peculiar behaviors have been observed in CTO, such as the lack of saturation of the magnetization up to 140 kOe [12], the occurrence of a minimum value of magnetization and anomalous specific heat peak at T_{comp} under $H = 50$ kOe [13], and the sign change of exchange-bias field from negative to positive at $T = 4$ K with the increase of cooling magnetic field [16], but no reasonable explanation was given for these unusual phenomena, and their correlation with SSG state is not clear. Nevertheless, we notice that similar scenarios were also found in some rare earth alloys [21,22], $RCr_{1-x}Fe_xO_3$ (R = some rare earth ion) [23–25], spinel $Co(Cr_{1-x}Fe_x)_2O_4$ [26,27], and Mn, Al-substituted $NiCr_2O_4$ [28,29]. It was reported that the moment of polarized conduction electron or rare earth ion leads to the

*liuxzh39@mail.sysu.edu.cn
†suiyu@hit.edu.cn

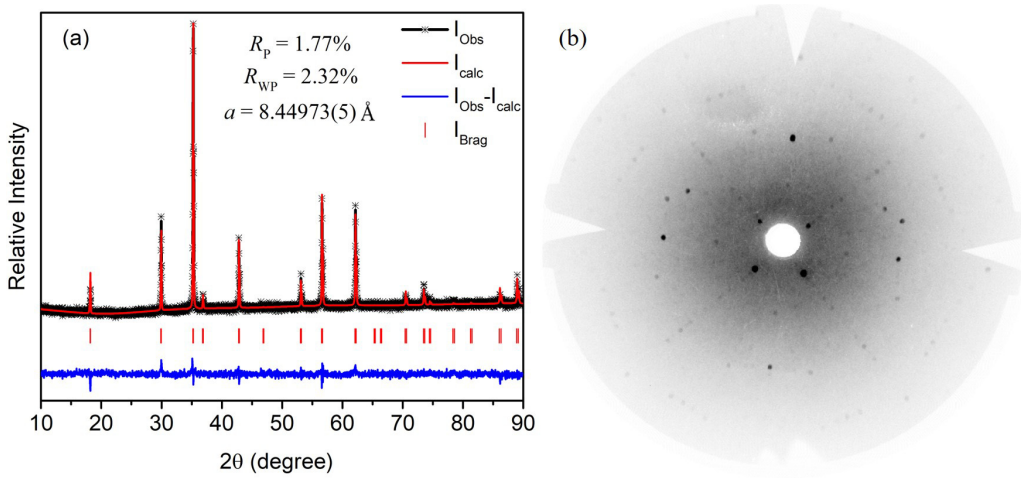

FIG. 1. (a) The room temperature x-ray powder diffraction patterns (plus marks) and Rietveld refinement result (solid lines) of CTO. (b) The Laue pattern taken from the CTO single crystal along the [100] direction.

exchange-bias effect and the unsaturated magnetization in rare earth alloys and $R\mathrm{Cr}_{1-x}\mathrm{Fe}_x\mathrm{O}_3$ [21–25], and the spin reorientation transition brings about the minimum value of magnetization at magnetic compensation temperature. However, different from $R\mathrm{Cr}_{1-x}\mathrm{Fe}_x\mathrm{O}_3$ [23–25] and rare earth alloys [21,22], it is absence of the extra moment (such as the moment of polarized conduction electron or rare earth ion) in spinel oxides except for the ferrimagnetic moment, and there is also no reasonable explanation for these anomalous properties in spinel chromates. Therefore, it is necessary to investigate again CTO with spinel structure to further understand the origin of these unusual behaviors in spinel oxides.

In this paper, we find a spin reorientation transition that occurs at $T_{\mathrm{comp}} \approx 31\,\mathrm{K}$ under magnetic field >20 kOe, in addition to the ferrimagnetic ordering transition at $T_C \approx 48\,\mathrm{K}$. By systematically measuring for different physical properties, we propose a phenomenological model to understand the anomalous phenomena in CTO. The magnetic structure of CTO is sensitive to the external magnetic field, and the oblique spin moments at B sites in CTO can be easily deflected by external magnetic field, bringing about a change of longitudinal component. Moreover, the variation of the longitudinal component and the spin reorientation transition at T_{comp} induced by strong magnetic field together lead to those anomalous properties at T_{comp} in CTO.

II. EXPERIMENT

Appropriate proportions of Co_3O_4 and TiO_2 were mixed and then calcined at 1100 °C for 24 h to synthesize the pure polycrystalline CTO. The polycrystalline powder was pressed into rods under 120 MPa hydrostatic pressure and then calcined again at 1120 °C for 12 h. The CTO single crystal was grown by the optical floating-zone technique in air. The growth rate was controlled to 5 mm/h and the feed and seed rods rotated in opposite directions at 20 rpm. Small pieces of single crystal were ground into fine powder to check the phase purity by x-ray diffraction (XRD), and Laue back reflection was used to determine the crystal principal axis. Zn_2TiO_4 (ZTO) polycrystals were also synthesized by high-temperature solid-phase reaction to estimate the lattice specific heat of CTO. The magnetization hysteresis loops $M(H)$, direct current (DC) magnetizations $M(T)$ and AC magnetic susceptibilities $\chi'(T)$, specific heat $C_P(T)$, thermal expansion $\Delta L/L_{80\,\mathrm{K}}$, and magnetostriction $\Delta L/L_0$ of CTO crystal were measured by using a physical property measurement system (PPMS). Thereinto, all measurements were performed with applying a magnetic field along the [100] direction of CTO crystal. Here, $M(T)$ and $\Delta L/L_{80\,\mathrm{K}}$ curves under different magnetic fields were recorded in zero-field-cooled (ZFC) and field-cooled (FC) procedures. Also, $M(H)$ and $\Delta L/L_0$ curves at different temperatures were recorded after a ZFC from 100 K, which is much higher than the magnetic ordering temperature T_C. Neutron powder diffraction (NPD) was carried out on a crushed CTO single crystal using the diffractometer Wombat available at ANSTO, employing a Ge (115) monochromator with wavelength configured to be 2.41 Å. The data were collected from 3.7 to 80 K by a step of 1 K during the warming process.

III. RESULTS

From the room temperature powder XRD pattern in Fig. 1(a), no impurity phase can be detected in our sample. The lattice parameter obtained from the Rietveld refinement with cubic structure (space group $Fd\text{-}3m$) is $a = 8.44973(5)$ Å, consistent with the structural data reported before [13]. The clear Laue diffraction spots along the [100] direction indicates the high quality of our crystal, as shown in Fig. 1(b).

Like previous papers [13–16], the DC magnetic susceptibilities $\chi(T)$ of CTO crystal along the [100] direction under $H = 100\,\mathrm{Oe}$ increase rapidly around $T_C \approx 48\,\mathrm{K}$ and exhibit a ferrimagnetic compensation behavior at $T_{\mathrm{comp}} \approx 31\,\mathrm{K}$, as shown in Fig. 2(a). The temperature dependence of the reciprocal of magnetic susceptibility $\chi^{-1}(T)$ in the FC process is displayed in Fig. 2(b). According to the molecular field theory of ferrimagnetism, the susceptibility was fitted by the

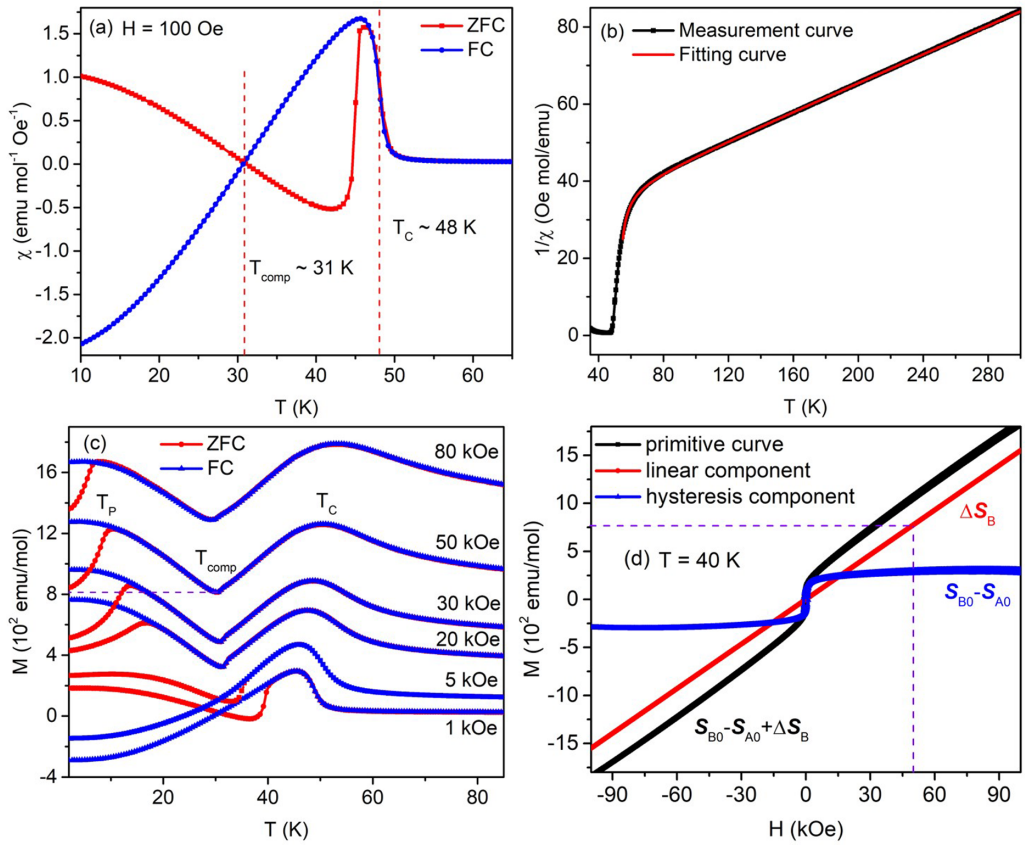

FIG. 2. (a) The temperature dependence of direct current (DC) magnetic susceptibility $M(T)$ of CTO crystal along the [100] direction at $H = 100$ Oe under zero-field-cooled (ZFC) and field-cooled (FC) measurement procedures. (b) Temperature variation of the inverse paramagnetic susceptibility $\chi^{-1}(T)$ in FC process. (c) The $M(T)$ curves under different magnetic fields in ZFC (red line) and FC (blue line) processes. (d) Magnetic hysteresis loop at $T = 40$ K under ZFC process, in which the black line is the primitive curve, the red line represents the linear component, and the blue line is the typical hysteresis loop that reaches saturation.

modified Curie-Weiss law [30],

$$\frac{1}{\chi} = \frac{T-\theta_a}{C} - \frac{\sigma_0}{T-\theta'}. \tag{1}$$

The red curve in Fig. 2(b) represents the fitting result using the data between 55 and 300 K, and the fitting parameters derived from the two-sublattice model of ferrimagnetism are $\theta_a = -154.7$ K, $C = 5.39$ emu K/mol, $\theta' = 51.7$ K, and $\sigma_0 = 51.3$ mol K/emu, respectively. The ratio of asymptotic Curie temperature θ_a to ferrimagnetic ordering temperature T_C is known as frustration factor [30], and the value of $f = \theta_a/T_C \approx 3.2$ suggests an appreciable magnetic frustration in CTO crystal. From the fitting parameter $C = N\mu_{\text{eff}}^2/3k_{\text{B}}$, the effective magnetic moment μ_{eff} is $\sim 6.56\,\mu_{\text{B}}$/f.u., close to the theoretical value of $\mu_{\text{eff}} \approx 6.48\,\mu_{\text{B}}$/f.u. calculated by using $\mu_{\text{eff}}^2 = \mu_T^2 + \mu_O^2$ [30,31], where the magnetic moments of Co^{2+}, Co^{3+}, and Ti^{3+} ions are $3.87\,\mu_{\text{B}}$ ($S = \frac{3}{2}$), $4.90\,\mu_{\text{B}}$ ($S = 2$), and $1.73\,\mu_{\text{B}}$ ($S = \frac{1}{2}$), respectively [13]. This confirms that the cation distribution of CTO is $(Co^{2+})_T[Co^{3+}Ti^{3+}]_O O_4$.

As shown in Fig. 2(c), with increasing the magnetic field, the magnetic compensation behavior of CTO disappears gradually, and then a minimum value of magnetization arises at T_{comp} under $H \geqslant 20$ kOe in ZFC and FC processes. The analogous phenomenon was observed in $Nd_{0.75}Ho_{0.25}Al_2$ [21] and $Co(Cr_{0.95}Fe_{0.05})_2O_4$ [26,27], in which a spin reorientation transition induced by magnetic field occurs at T_{comp}. Thus, these results indicate the spin reorientation transition also occurs at T_{comp} in CTO under high magnetic field >20 kOe. Furthermore, $M(T)$ curves in ZFC and FC processes overlap over a wide temperature range, but separate from each other at lower temperature, marked as T_P, which decreases rapidly with increasing magnetic field. In addition, the magnetization below T_C increases linearly with magnetic field, but cannot reach the saturation, even at a magnetic field >100 kOe, as shown in Fig. 2(d). The magnetic hysteresis loop at $T = 40$ K can be separated into two components, a linear component and a typical hysteresis loop, suggesting that the magnetization of CTO is contributed by two components with different origins.

As shown in Figs. 3(a)–3(d), the AC magnetic susceptibility $\chi'(T)$ curve with a flat sample parallel to the magnetic field exhibits a sharp peak with an obvious frequency-dependent characteristic at ~47.6 K, a minimal value at $T_{\text{comp}} \approx 31$ K, and a broad peak at $T_P \approx 16.5$ K. However, under static magnetic field $H = 200$ Oe, the peak of $\chi'(T)$ at ~47.6 K splits into two parts: a peak at 48.2 K and a shoulder at 46.5 K. The peak is independent on the frequency, meaning a ferrimagnetic ordering transition at $T_C \approx 48.2$ K, while the shoulder is sensitive to the frequency. Like the observations by Srivastava *et al.* [20], the sharp peak at 48.2 K and the

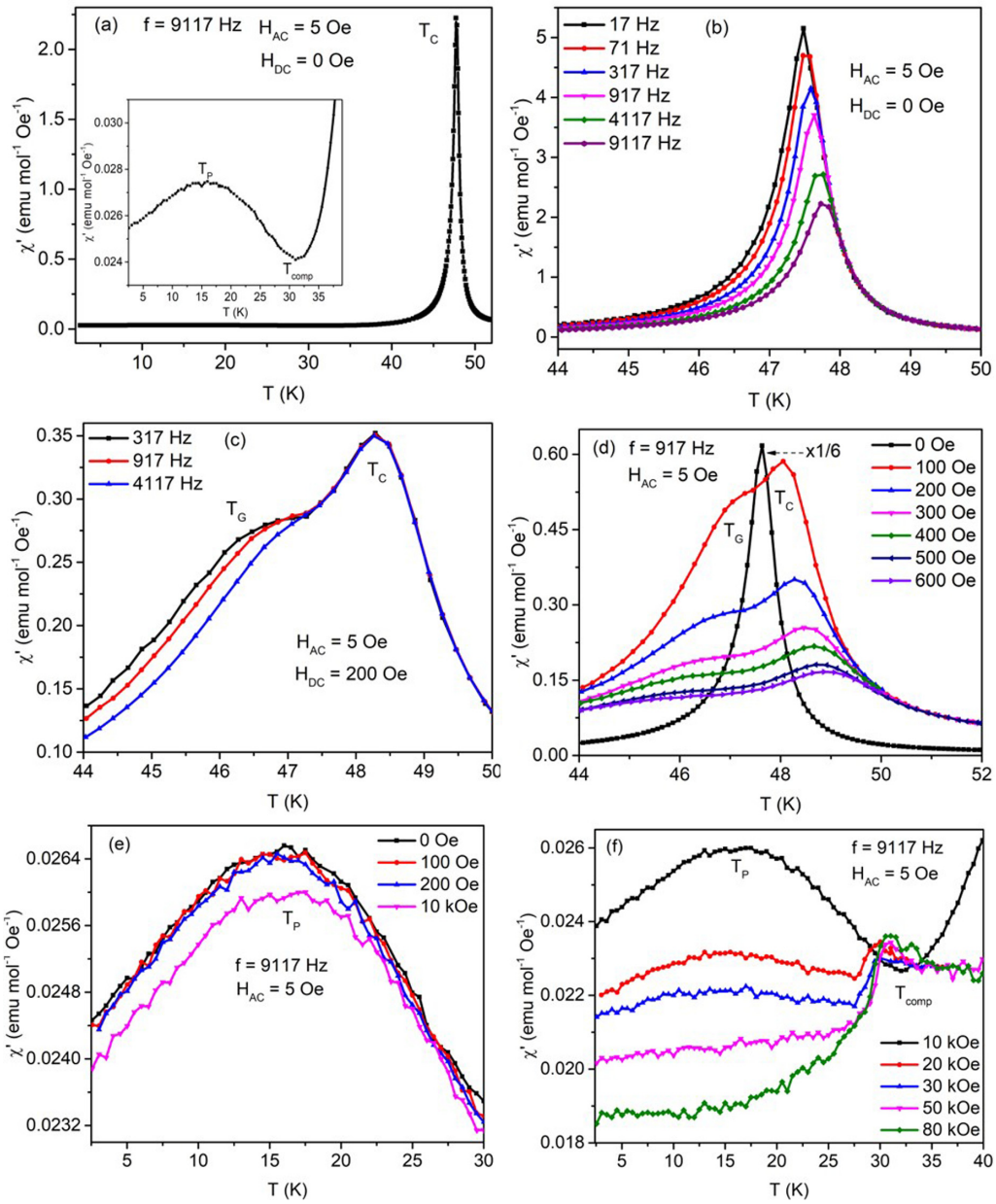

FIG. 3. (a) The $\chi'(T)$ curve of CTO crystal along the [100] direction. The inset is a magnification at low temperature. (b) and (c) The $\chi'(T)$ curves at different frequencies near T_C under $H_{DC} = 0$ and 200 Oe, respectively. (d) The $\chi'(T)$ curves near T_C under different magnetic fields H_{DC}. (e) and (f) The $\chi'(T)$ curves near T_P under $H_{DC} < 10$ kOe and $H_{DC} > 10$ kOe, respectively.

shoulder at 46.5 K are both suppressed with increasing static magnetic field.

The NPD patterns of CTO were collected on the instrument Wombat. The magnetic scattering signal at lower temperature can be obtained by subtraction of the NPD data at 75 K, at which the short-range ordering peak extinguishes, as shown in Fig. 4(a). Some other magnetic peaks appear below T_C, as shown in Fig. 4(b). The most prominent peak $(111)_M$ refection appears ~29 °. The other prominent magnetic contributions include $(022)_M \sim 48°$, $(400)_M \sim 70°$, and $(133)_M \sim 78°$, which all are indicative of a ferrimagnetic structure between A and B sites along the a axis, as previous reported [18,32]. Moreover, a weak but unambiguous $(200)_M$ reflection was also observed in our experiment, which signifies an antiferromagnetic transverse component perpendicular to the ferrimagnetic component [12,18]. Although the peak width is broad and not ideally suitable for a Rietveld refinement, a fitting procedure using FULLPROF was attempted to extract the magnetic structure and moment size. To account for the broad profile of the magnetic peak, a Lorentzian function was used to have a better fit. During refinement, the moment size of Co^{3+} and Ti^{3+} were constrained to be 4:1 due to the t_{3g}^4 and t_{3g}^1 orbital configurations. The fitting magnetic moment of Co^{2+} at the A site and Co^{3+} and Ti^{3+} at the B site are determined to be -1.61, 3.25, and 0.81 μ_B, respectively, which are close to the previous report [18].

The temperature dependence of the intensity for $(111)_M$, $(022)_M$, and $(200)_M$ reflections are presented in Fig. 4(c).

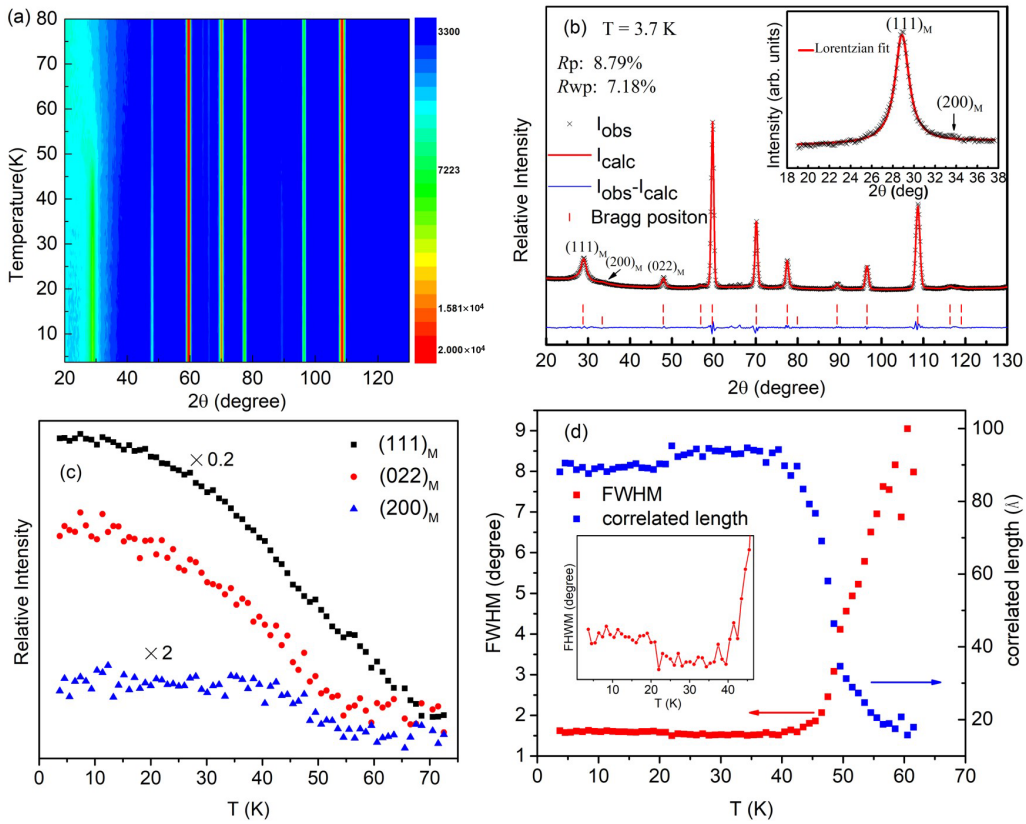

FIG. 4. (a) The contour plot for the neutron powder diffraction (NPD) data of CTO <80 K. (b) Rietveld refinements of the NPD data at $T = 3.7$ K. The insets present the prominent magnetic reflections $(111)_M$ and $(200)_M$ in enlarged form, which are fitted using the Lorentz function. (c) The dependence of relative intensities of $(111)_M$, $(022)_M$, and $(200)_M$ peaks on temperature. (d) The dependence of full width (red dots) at half maximum (FWHM) of the magnetic reflection $(111)_M$ and correlation length (blue dots) on temperature. The insets present the FWHM in enlarged form < 45 K.

Here, the $(022)_M$ and $(200)_M$ peaks begin to appear when temperature ∼50 K, namely, near T_C, but the $(111)_M$ reflection retains up to ∼70 K with a long tail, indicating the short-range ordering appears ∼70 K far above the T_C. Meanwhile, the strongest magnetic peak $(111)_M$ reflection can be perfectly fitted by a pure Lorentzian function, as shown in the inset of Fig. 4(b), and it is remarkably broader than the nuclear reflection, suggesting the existence of short-range ordering in CTO. Moreover, the full width at half maximum (FWHM) of the $(111)_M$ peak also shows a very unusual feature with temperature. One can see from Fig. 4(d) that the FWHM of the $(111)_M$ peak decreases quickly when temperatures decreases from T_C; however, it shows a slight increase <20 K, which is near the temperature T_P where a local AC susceptibility maximum is observed. The increase of FWHM signifies a reduced correlation length of the spin ordering ($\xi = 2\pi/\mathrm{FWHM}_{[111]}$) < 20 K.

In Figs. 3(e) and 3(f), the $\chi'(T)$ curves show a sharp drop at T_{comp} under $H \geqslant 20$ kOe, instead of the minimum at zero field, which is also caused by the spin reorientation transition at T_{comp} by the magnetic field. In zero field, a broad hump in $\chi'(T)$ is also observed around $T_P \approx 16.5$ K, which remains unchanged up to $H = 200$ Oe. However, when the magnetic field increases further, this hump is suppressed gradually and disappears under $H \geqslant 50$ kOe, as shown in Fig. 3(f). Qualitatively, the value of AC susceptibility reflects the response rate of the magnetic moment to the external magnetic field, and the larger $\chi'(T)$ corresponds to a larger spin moment or a spin which is easier to rotate in phase with the external field. The absolute value of $M(T)$ increases monotonously below T_{comp}, showing the net moment increases with lowering temperature. Nevertheless, the magnitude of $\chi'(T)$ rather shows a decrease below T_P, implying a freezing of spin moment below T_P. This result is consistent with the abnormal increase of FWHM of the $(111)_M$ peak in NPD patterns <20 K, suggesting that further disordering or freezing of spin moments may occur below T_P.

In addition to these unusual magnetic phenomena shown above, some other special physical properties are also induced at T_{comp} by magnetic field >20 kOe in CTO. Inverse spinel CTO and ZTO have the same crystal structure [33,34], and ZTO is nonmagnetic. Thus, the lattice specific heat of CTO can be estimated by that of ZTO; that is, $C_P(T)_{\mathrm{CTO}} = \sqrt{M_{\mathrm{CTO}}/M_{\mathrm{ZTO}}}C_P(T)_{\mathrm{ZTO}}$. Here, $C_P(T)_{\mathrm{CTO}}$ and $C_P(T)_{\mathrm{ZTO}}$ are the lattice specific heat of CTO and ZTO, and M_{CTO} and M_{ZTO} are the relative molecular mass of CTO and ZTO, respectively. The scaling factor $\sqrt{M_{\mathrm{CTO}}/M_{\mathrm{ZTO}}} = 0.973$. As displayed in Fig. 5(a), the magnetic specific heat of CTO can be obtained by deducting the lattice contribution. A weak specific heat peak appears at ferrimagnetic ordering temperature $T_C \approx 48$ K, but no specific heat anomaly can be found at T_{comp} under zero field. The entropy change ΔS_E was

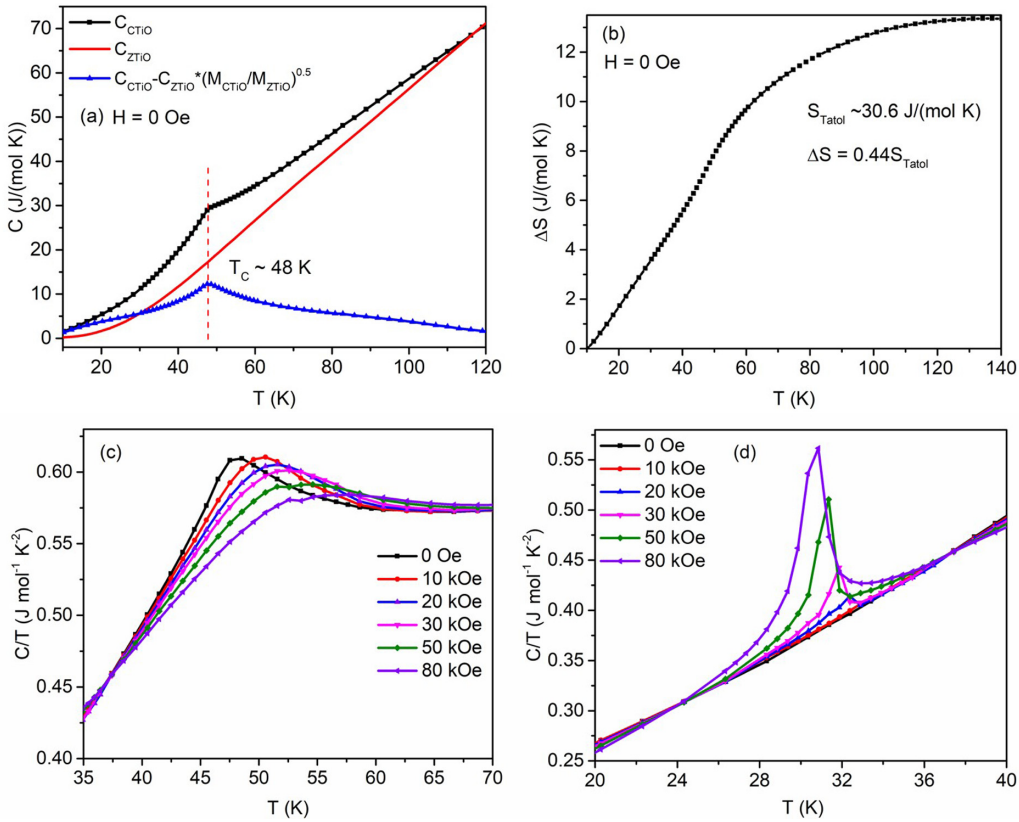

FIG. 5. (a) The total specific heat (black square) and magnetic specific heat (blue triangle) of CTO crystal under zero field. The specific heat of the lattice is subtracted by using the specific heat of ZTO (red line). (b) The change of entropy between 10 and 140 K under zero field. (c) and (d) The specific heats under different magnetic fields near T_C and $T_{\rm comp}$, respectively.

calculated to be 13.4 J/(mol K) between 10 and 140 K by using the formula $\Delta S_E = \int_{T1}^{T2} \frac{C_m}{T} dT$. The spin quantum number of Co^{2+}, Co^{3+}, and Ti^{3+} ions are $\frac{3}{2}$, $\frac{4}{2}$, and $\frac{1}{2}$, respectively. Thus, in theory, the total magnetic entropy change of CTO should be $S_E = R\ln(2\times\frac{3}{2}+1) + R\ln(2\times\frac{4}{2}+1) + R\ln(2\times\frac{1}{2}+1) \approx 30.7\,\mathrm{J/(mol\,K)}$ in the case of complete magnetic ordering, where R is the universal gas constant. It is evident that $S_E \gg \Delta S_E$, estimated between 10 and 140 K, indicating again the incomplete magnetic ordering in CTO below T_C, which is also consistent with the small spin correlation length derived from NPD. As shown in Fig. 5(c), with increasing magnetic field, the specific heat peak at T_C is suppressed gradually. A sharp specific heat peak emerges around $T_{\rm comp}$ under $H = 20$ kOe in Fig. 5(d) and raises rapidly as the magnetic field increases, though there is no obvious anomaly in the specific heat curves <20 kOe. It is worth noting that the critical magnetic fields, at which the abnormal specific heat peak, the minimum value of $M(T)$, and the drop of $\chi'(T)$ begin to appear, are all close to each other, implying that there should be some intrinsic correlation behind these phenomena.

This correlation was further confirmed by using the strain measurement depending on temperature and magnetic field, as shown in Figs. 6(a)–6(d). The strain under zero field begins to deviate from the linear decrease at ~60 K, which is beyond the ferrimagnetic ordering temperature, suggesting that the short-range magnetic ordering emerges far above T_C. Though there is no obvious transition in the $\Delta L/L_{80\,\mathrm{K}}$ curve under zero field, the thermal expansion coefficient $\alpha(T) = d[\Delta L(T)/L_{80\,\mathrm{K}}]/dT$ exhibits a typical λ peak at T_C in Fig. 6(b), further confirming the nature of magnetic ordering transition. The $\alpha(T)$ curve also exhibits two discontinuous changes at $T_{\rm comp}$ and T_P, suggesting the occurrence of weak lattice distortion at these two temperatures. In ZFC and FC processes, like the variation of specific heat, there is no obvious strain anomaly around $T_{\rm comp}$ under $H < 20$ kOe, but a sharp jump of $\Delta L/L_{80\,\mathrm{K}}$ happens just under magnetic field >20 kOe. Then this jump at $T_{\rm comp}$ is enhanced with further increasing magnetic field, implying that the lattice distortion induced by the magnetic field should be responsible for the anomalous specific heat peak at $T_{\rm comp}$ under $H \geqslant 20$ kOe. In addition, being consistent with the separation of $M(T)$ curves in ZFC and FC processes, $\Delta L/L_{80\,\mathrm{K}}$ curves exhibit a drop again below T_P under $H \geqslant 20$ kOe in ZFC process, but no change in FC process. As shown in Figs. 7(a) and 7(b), the CTO crystal exhibits a positive magnetostriction below $T_{\rm comp}$ but a negative magnetostriction above $T_{\rm comp}$. Apparently, the lattice distortion at $T_{\rm comp}$ under the strong magnetic field should be caused by the opposite magnetostriction behavior above $T_{\rm comp}$ and below $T_{\rm comp}$.

Though Nayak *et al.* [13–15] reported some unusual phenomena in CTO, no clear interpretation was given. In this paper, some anomalous behaviors were further observed in CTO, including the drop of $\chi'(T)$, the large lattice distortion, and the opposite magnetostriction behavior at $T_{\rm comp}$ under strong magnetic fields. More importantly, these unusual phenomena have the same critical field, implying that they could be closely

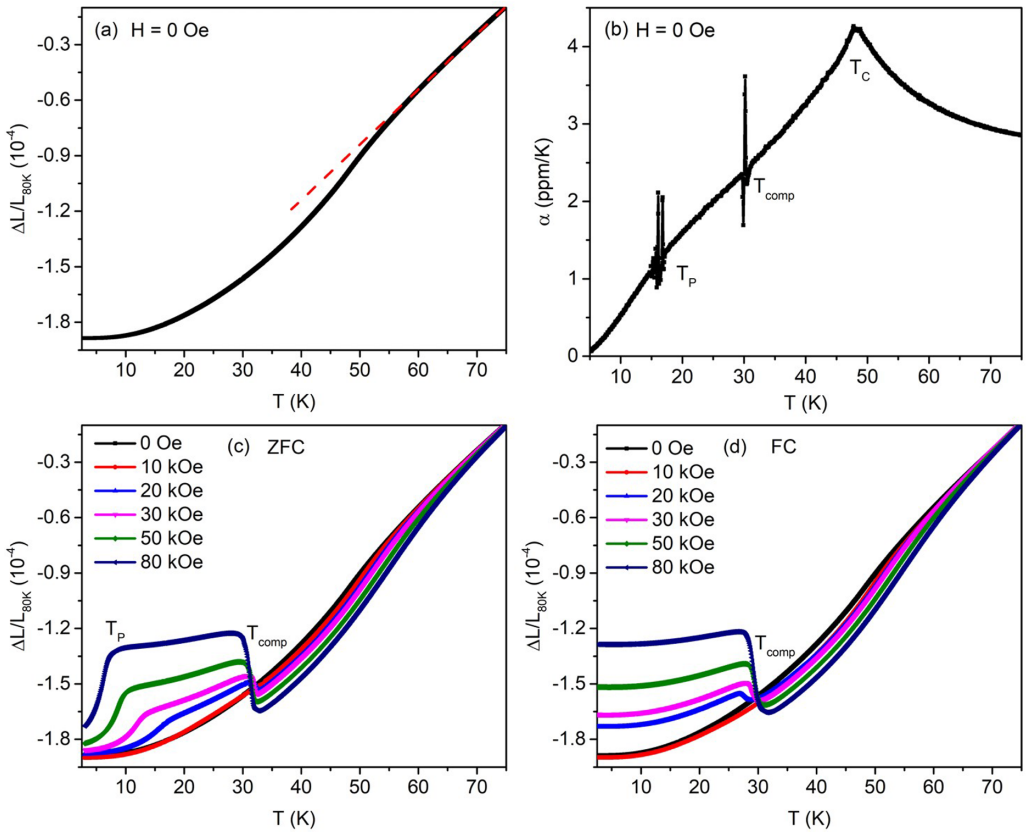

FIG. 6. $H \parallel L$. (a) and (b) The thermal expansion and thermal expansion coefficient of CTO single crystal under zero field. (c) and (d) The thermal expansions under different magnetic fields in zero-field-cooled (ZFC) and field-cooled (FC) processes, respectively.

related with the evolution of the magnetic structure of CTO under magnetic field. Therefore, we proposed a phenomenological model in the next section to understand the mechanism behind these anomalous phenomena in CTO crystal.

IV. DISCUSSIONS

The results of magnetism and neutron diffraction in Sec. III prove that the magnetic ground state of CTO consists of a longitudinal ferrimagnetic component along the a axis and a transverse component in the bc plane. Inspired by the noncollinear (Yafet-Kittel) ferrimagnetic ordering in spinel systems [6], we proposed a schematic diagram in Fig. 8(a) based on experimental results above to show the change of the magnetic structure in CTO with magnetic field parallel to the a axis. There is an angle θ between the spin moments at B sites (black arrow) and the a axis in CTO. The spin moments at A sites along the a axis (red arrow) and the longitudinal components of spins at B sites (blue arrow) are antiparallel to each other, leading to a ferrimagnetic ordering along the a

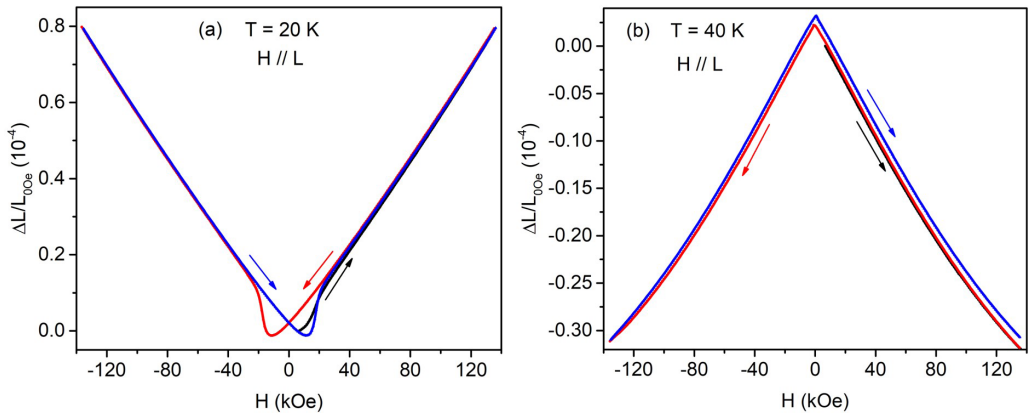

FIG. 7. $H \parallel L$. (a) and (b) The magnetostrictions after zero-field-cooled (ZFC) process at $T = 20$ and 40 K, respectively. The black line is the initial magnetostriction, and the red and blue lines are the curves in falling and rising field processes, respectively.

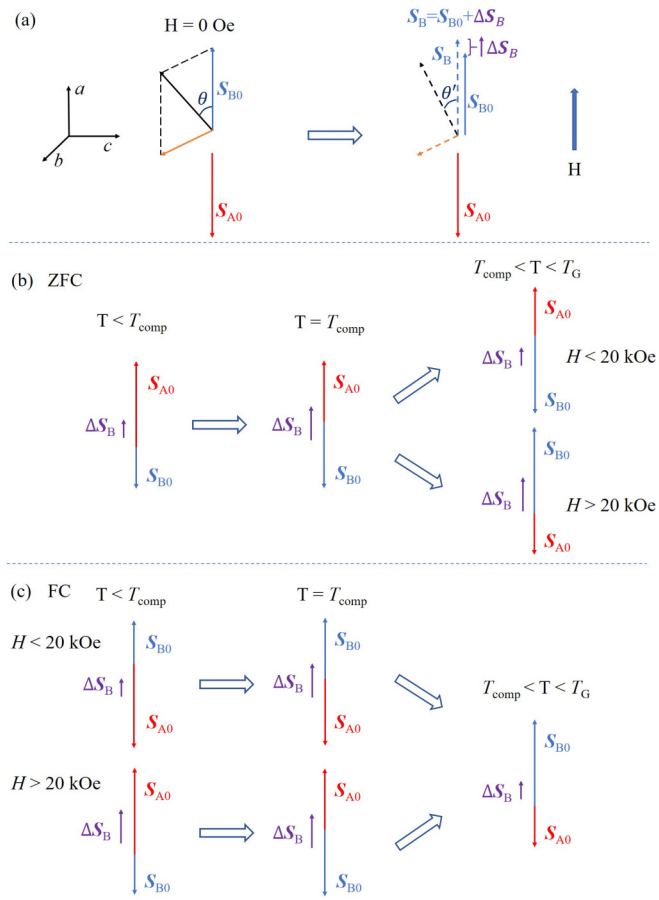

FIG. 8. (a) The inferred spin structure of CTO crystal. There is an angle θ between the spin moments at B sites (black arrow) and the a axis (the direction of magnetic field). The spin moments at A sites ($\mathbf{S}_{A0}$, red arrow) and the longitudinal components of spins at B sites ($\mathbf{S}_{B0}$, blue arrow) are antiparallel to each other, leading to a ferrimagnetic ordering. The transverse components of spins at B sites (yellow arrow) randomly point to different directions in the bc plane, contributing to the spin glass behavior. Under the external magnetic field, the oblique spins are easily deflected, resulting in the changes of angle θ and bringing about a variation of the longitudinal components $\Delta\mathbf{S}_B = \mathbf{S}_B - \mathbf{S}_{B0}$ (violet arrow). (b) and (c) The dependence on temperature of longitudinal spin components in zero-field-cooled (ZFC) and field-cooled (FC) processes, respectively.

axis. However, different from Yafet-Kittel ordering, the transverse components of spins at B sites in CTO (yellow arrow) exhibit a short correlation length.

The angle θ in Yafet-Kittel ordering is hard to be deflected by the external magnetic field due to the strong exchange coupling in spinel. However, the spins at B sites are not very stable in CTO due to the competition between interactions of spins at B sites $J^{3+}_{Co}-^{3+}_{Co}$, $J^{3+}_{Ti}-^{3+}_{Ti}$, and $J^{3+}_{Co}-^{3+}_{Ti}$. Therefore, the oblique spin at B sites may be easily deflected by an external magnetic field parallel to the a-axis direction, leading to the change of angle θ and then the magnitude of longitudinal and transverse components, as displayed in Fig. 8(a). Because only the longitudinal components along the magnetic field direction directly contribute to the measured magnetization, we merely consider the longitudinal components in the following analysis to make the picture more concise.

When applying the magnetic field along the a axis, the variation of the longitudinal components at B sites can be written as $\Delta\mathbf{S}_B = \mathbf{S}_B - \mathbf{S}_{B0}$. Here, vectors $\mathbf{S}_B$ and $\mathbf{S}_{B0}$ are the longitudinal component of the spins at the B site with and without magnetic field, respectively. Because $\mathbf{S}_A$ is (anti)parallel to the magnetic field direction, the variation of $\mathbf{S}_{A0}$ can be negligible under magnetic field; that is, $\mathbf{S}_A = \mathbf{S}_{A0}$. It needs to be emphasized that $\Delta\mathbf{S}_B$ has two obvious characteristics. First, $\Delta\mathbf{S}_B$ is always parallel to the direction of external magnetic field since the oblique spins always deflect toward the magnetic field. Second, there is an antiferromagnetic interaction between $\Delta\mathbf{S}_B$ and $\mathbf{S}_{A0}$ because the magnetic interaction between $\mathbf{S}_{B0}$ and $\mathbf{S}_{A0}$ is always antiferromagnetic in spinel systems. The total longitudinal spin moment under magnetic field can be described by $\mathbf{S}_B + \mathbf{S}_A = \mathbf{S}_{B0} + \Delta\mathbf{S}_B + \mathbf{S}_{A0} = \Delta\mathbf{S}_B + (\mathbf{S}_{B0} + \mathbf{S}_{A0})$. Therefore, the magnetization per mole CTO is $\mathbf{M} = N_A g\mu_B(\mathbf{S}_B + \mathbf{S}_A) = N_A g\mu_B \Delta\mathbf{S}_B + N_A g\mu_B(\mathbf{S}_{B0} + \mathbf{S}_{A0})$, which can be divided into two parts, the spontaneous magnetization under zero field $N_A g\mu_B(\mathbf{S}_{B0} + \mathbf{S}_{A0})$ and the magnetization variation $N_A g\mu_B \Delta\mathbf{S}_B$ induced by the magnetic field. Here, N_A is the Avogadro constant, g is the Lande factor, and μ_B is the Bohr magneton.

It is well known that the magnetic compensation behavior in CTO originates from the different variation rates of the magnetic moments at A and B sites with temperature, according to the molecular field theory in spinel. Here, $|\mathbf{S}_{A0}| > |\mathbf{S}_{B0}|$ in CTO below T_{comp} based on the NPD results by Thota *et al.* [18]. Thus, from the magnetic compensation behavior shown in Fig. 2(a), $|\mathbf{S}_{A0}|$ should be $< |\mathbf{S}_{B0}|$ above T_{comp}, and equal to $|\mathbf{S}_{B0}|$ at $T = T_{comp}$ in CTO. Therefore, the schematic diagrams in Figs. 8(b) and 8(c) demonstrate the spin component dependence on temperature in FC and ZFC processes, respectively. The deflection of oblique spins is very small under low field, and then the contribution of $\Delta\mathbf{S}_B$ on magnetization is negligible, so a normal magnetic compensation behavior originating from $|\mathbf{S}_{B0}| = |\mathbf{S}_{A0}|$ can be observed at T_{comp} under $H \leqslant 1$ kOe, in which the magnetizations in ZFC and FC processes are both zero at T_{comp}, as shown in Figs. 2(a) and 2(c).

Though $\mathbf{S}_{B0} + \mathbf{S}_{A0}$ keeps always zero at T_{comp}, $\Delta\mathbf{S}_B$ increases gradually with magnetic field, contributing a non-negligible magnetization $N_A g\mu_B \Delta\mathbf{S}_B$ under high field. Thus, the magnetic compensation behavior disappears under high field >5 kOe, as displayed in Fig. 2(c). The magnetization is ~814 emu/mol at T_{comp} under $H = 50$ kOe in the $M(T)$ curve in Fig. 2(c), which is near the value (~756 emu/mol) of the linear magnetization under $H = 50$ kOe at 40 K in Fig. 2(d). Therefore, the linear increase of magnetization under high field and the magnetization at T_{comp} should both represent the contribution of $\Delta\mathbf{S}_B$.

In addition to enhancing $\Delta\mathbf{S}_B$, the strong magnetic field can also bring about a spin reorientation transition in CTO. We know that the net magnetic moment always tends to align in the magnetic field direction. Under low field, the magnetization is a negative value above (below) T_{comp} in ZFC (FC) process. Thus, the longitudinal component is unstable above (below) T_{comp} in the ZFC (FC) process since $\mathbf{S}_{B0} + \mathbf{S}_{A0}$ is antiparallel to $\boldsymbol{H}$, and then it prefers to rotate 180° to reduce the magnetic energy when the external magnetic field is enough

strong. Thus, as shown in Figs. 8(b) and 8(c), a spin reorientation transition at T_{comp} can be induced by the magnetic field > 20 kOe, which further leads to a positive magnetization ($\mathbf{S}_{B0} + \mathbf{S}_{A0}$ is parallel to $\mathbf{H}$) for $T > T_{comp}(T < T_{comp})$ in the ZFC (FC) process. Consequently, a minimum value of magnetization can be observed at T_{comp} under high field instead of the magnetic compensation behavior under low field.

It needs to be emphasized that $\Delta\mathbf{S}_B$ reflects the influence of magnetic field on antiferromagnetic interaction energy between $\mathbf{S}_{A0}$ and $\mathbf{S}_B$. According to the Heisenberg Hamilton $E = -J\mathbf{S}_i \cdot \mathbf{S}_j$, we mark the antiferromagnetic interaction energy between $\mathbf{S}_{A0}$ and $\mathbf{S}_{B0}$ as $E_0 = -J\mathbf{S}_{A0} \cdot \mathbf{S}_{B0}$ under zero field. Here, J is the antiferromagnetic exchange-interaction constant ($J < 0$). With increasing magnetic field, the energy E_0 will change to $E_{\mathrm{H}} = -J\mathbf{S}_A \cdot \mathbf{S}_B = -J\mathbf{S}_{A0}(\mathbf{S}_{B0} + \Delta\mathbf{S}_B) = E_0 - J\mathbf{S}_{A0} \cdot \Delta\mathbf{S}_B = E_0\Delta E$. Here, $\Delta E = -J\mathbf{S}_{A0} \cdot \Delta\mathbf{S}_B$ represents the antiferromagnetic interaction energy between $\mathbf{S}_{A0}$ and $\Delta\mathbf{S}_B$.

Generally, the magnetic system always tends to the lower energy state after the ferrimagnetic ordering transition. Therefore, a spontaneous negative magnetostriction will occur under zero field to lower energy $E_0 = -J\mathbf{S}_{A0} \cdot \mathbf{S}_{B0}$ because the smaller the ion distance, the larger exchange-interaction constant J. As shown in Fig. 6(a), CTO exhibits an obvious lattice shrinkage under zero field; that is, the slope of the $\Delta L/L_{80\,\mathrm{K}}$ curve increases after ferrimagnetic ordering. Compared with that under zero field, $\Delta E = -J\mathbf{S}_{A0} \cdot \Delta\mathbf{S}_B$ will cause an extra magnetostriction under high field after the ferrimagnetic ordering transition. If ΔE is a negative (positive) value, it will lead to a lattice shrinkage (expansion). Under high field, $\Delta\mathbf{S}_B$ is always antiparallel to $\mathbf{S}_{A0}$ above T_{comp}, indicating that ΔE is also a negative value. Hence, CTO exhibits a negative magnetostriction above T_{comp}, as shown in Fig. 7(b). On the contrary, $\Delta\mathbf{S}_B$ is parallel to $\mathbf{S}_{A0}$ below T_{comp} under high field > 20 kOe, due to the spin reorientation transition induced by magnetic field. Thus, ΔE is a positive value, leading to a positive magnetostriction below T_{comp}, as shown in Fig. 7(a). Therefore, the opposite magnetostriction above and below T_{comp} originates from the spin reorientation transition at T_{comp} under $H \geqslant 20$ kOe, which causes the arrangement state between $\Delta\mathbf{S}_B$ and $\mathbf{S}_{A0}$ changing from antiparallel above T_{comp} to parallel below T_{comp}.

Therefore, due to the opposite magnetostriction effect above and below T_{comp}, an obvious jump of strain was observed at T_{comp} under $H \geqslant 20$ kOe, which also brings about the occurrence of an anomalous specific heat peak at T_{comp} due to the release of lattice distortion energy. With increasing the magnetic field, $\Delta\mathbf{S}_B$ increases, and then the magnetostriction is also enhanced, further causing the stronger jump of strain and specific heat peak at T_{comp}.

All the anomalous phenomena above in CTO can be understood by the spin moment being susceptible to the external magnetic field at B sites and the variation of the longitudinal ferrimagnetic component $\Delta\mathbf{S}_B$ induced by magnetic field, indicating that our model is self-consistent. Moreover, similar anomalous phenomena to those in CTO, such as the linearly increasing magnetization with magnetic field and the anomalous specific heat peak at magnetic compensation temperature, were also observed in $Co(Cr_{1-x}Fe_x)_2O_4$ [26,27]. These indicate our phenomenological model is not only applicable to CTO but also can be extended to other spinel oxides, which is important to understand the intrinsically complex magnetic behaviors in spinel systems.

V. CONCLUSIONS

In conclusion, CTO exhibits a complex magnetic structure below ferrimagnetic ordering temperature, consisting of a ferrimagnetic-ordered longitudinal component and a transverse component susceptible to the external magnetic field. The oblique spin moments at B sites can be easily deflected by magnetic field, leading to a variation of the longitudinal ferrimagnetic component $\Delta\mathbf{S}_B$. Moreover, when magnetic field exceeds 20 kOe, the longitudinal ferrimagnetic component antiparallel to the magnetic field direction can be flipped by 180 °, exhibiting a spin reorientation transition at T_{comp}. Together with $\Delta\mathbf{S}_B$, this transition plays an essential role in bringing about these anomalous phenomena in CTO crystal, including the minimum value of $M(T)$, the drop of $\chi'(T)$, the step of $\Delta L/L_{80\,\mathrm{K}}$, the sharp specific heat peak, and the sign change of magnetostriction above and below T_{comp}.

ACKNOWLEDGMENTS

The authors are grateful to Dr. Chin-Wei Wang in the National Synchrotron Radiation Research Center, Taiwan, for the help about the NPD measurement on the high-intensity diffractometer Wombat at the Australian Centre for Neutron Scattering (ACNS) of ANSTO. This paper is supported by the Funds for International Cooperation and Exchange of the National Natural Science Foundation of China (No. 51861135308), and Beijing National Laboratory for Condensed Matter Physics. Funded by Natural Science Foundation of Guangdong Province, China (No. 2021A1515010346) and Supported by the Guangdong-Hong Kong-Macao Joint Laboratory for Neutron Scattering Science and Technology.

[1] Y. J. Choi, J. Okamoto, D. J. Huang, K. S. Chao, H. J. Lin, C. T. Chen, M. van Veenendaal, T. A. Kaplan, and S.-W. Cheong, Phys. Rev. Lett. **102**, 067601 (2009).

[2] L. Rossi, A. Bobel, S. Wiedmann, R. Küchler, Y. Motome, K. Penc, N. Shannon, H. Ueda, and B. Bryant, Phys. Rev. Lett. **123**, 027205 (2019).

[3] T. Suzuki and T. Katsufuji, Phys. Rev. B **77**, 220402(R) (2008).

[4] Y. Nii, H. Sagayama, H. Umetsu, N. Abe, K. Taniguchi, and T. Arima, Phys. Rev. B **87**, 195115 (2013).

[5] Y. Nii, N. Abe, K. Taniguchi, and T. Arima, Appl. Phys. Lett. **100**, 051905 (2012).

[6] Y. Yafet and C. Kittel, Phys. Rev. **87**, 290 (1952).

[7] J.-H. Chung, Y.-S. Song, J.-H. Kim, T. Suzuki, T. Katsufuji, M. Matsuda, and S.-H. Lee, Phys. Rev. B **88**, 094430 (2013).

[8] A. V. Pronin, M. Uhlarz, R. Beyer, T. Fischer, J. Wosnitza, B. P. Gorshunov, G. A. Komandin, A. S. Prokhorov, M. Dressel, A. A. Bush, and V. I. Torgashev, Phys. Rev. B **85**, 012101 (2012).

[9] R. Nirmala, K.-H. Jang, H. Sim, H. Cho, J. Lee, N.-G. Yang, S. Lee, R. M. Ibberson, K. Kakurai, M. Matsuda, S.-W. Cheong, V. V. Gapontsev, S. V. Streltsov, and J.-G. Park, J. Phys.: Condens. Matter **29**, 13LT01 (2017).

[10] M. Hemmida, H. A. Krug von Nidda, V. Tsurkan, and A. Loidl, Phys. Rev. B **95**, 224101 (2017).

[11] G. J. Nilsen, Y. Okamoto, T. Masuda, J. Rodriguez-Carvajal, H. Mutka, T. Hansen, and Z. Hiroi, Phys. Rev. B **91**, 174435 (2015).

[12] J. Hubsch and G. Gavoille, Phys. Rev. B **26**, 3815 (1982).

[13] S. Nayak, S. Thota, D. C. Joshi, M. Krautz, A. Waske, A. Behler, J. Eckert, T. Sarkar, M. S. Andersson, R. Mathieu, V. Narang, and M. S. Seehra, Phys. Rev. B **92**, 214434 (2015).

[14] S. Nayak, K. Dasari, D. C. Joshi, P. Pramanik, R. Palai, A. Waske, R. N. Chauhan, N. Tiwari, T. Sarkar, and S. Thota, J. Appl. Phys. **120**, 163905 (2016).

[15] S. Nayak, D. C. Joshi, M. Krautz, A. Waske, J. Eckert, and S. Thota, J. Appl. Phys. **119**, 043901 (2016).

[16] A. Wei, S. Tao, Y. Fang, Z. D. Han, B. Qian, X. F. Jiang, H. Zhou, R. J. Tang, and D. H. Wang, J. Magn. Magn. Mater. **441**, 361 (2017).

[17] J. Villain, Z. Physik B **33**, 31 (1979).

[18] S. Thota, M. Reehuis, A. Maljuk, A. Hoser, J.-U. Hoffmann, B. Weise, A. Waske, M. Krautz, D. C. Joshi, S. Nayak, S. Ghosh, P. Suresh, K. Dasari, S. Wurmehl, O. Prokhnenko, and B. Büchner, Phys. Rev. B **96**, 144104 (2017).

[19] C. Liu, X. Kan, X. Liu, Z. Zhang, and J. Hua, Phys. Chem. Chem. Phys. **22**, 20929 (2020).

[20] J. K. Srivastava, J. A. Kulkarni, S. Ramakrishnan, S. Singh, V. R. Marathe, G. Chandra, V. S. Darshane, and R. Vijayaraghavan, J. Phys. C: Solid State Phys. **20**, 2139 (1987).

[21] P. D. Kulkarni, A. Thamizhavel, V. C. Rakhecha, A. K. Nigam, P. L. Paulose, S. Ramakrishnan, and A. K. Grover, Europhys. Lett. **86**, 47003 (2009).

[22] P. D. Kulkarni, S. K. Dhar, A. Provino, P. Manfrinetti, and A. K. Grover, Phys. Rev. B **82**, 144411 (2010).

[23] L. Wang, L. L. Zhang, X. Zhang, M. L. Zhong, Z. C. Zhong, and G. H. Rao, Ceram. Int. **45**, 6143 (2019).

[24] I. Fita, R. Puzniak, A. Wisniewski, and V. Markovich, Phys. Rev. B **100**, 144426 (2019).

[25] I. Fita, A. Wisniewski, R. Puzniak, E. E. Zubov, V. Markovich, and G. Gorodetsky, Phys. Rev. B **98**, 094421 (2018).

[26] R. Padam, S. Pandya, S. Ravi, A. K. Nigam, S. Ramakrishnan, A. K. Grover, and D. Pal, Appl. Phys. Lett. **102**, 112412 (2013).

[27] R. Padam, S. Pandya, S. Ravi, S. Ramakrishnan, A. K. Nigam, A. K. Grover, and D. Pal, J. Phys.: Condens. Matter **29**, 055803 (2017).

[28] J. Barman and S. Ravi, J. Mater. Sci. **53**, 7187 (2018).

[29] J. Barman and S. Ravi, J. Magn. Magn. Mater. **426**, 82 (2017).

[30] R. Nepal, Q. Zhang, S. Dai, W. Tian, S. E. Nagler, and R. Jin, Phys. Rev. B **97**, 024410 (2018).

[31] Q. S. Fu, X. H. Chen, C. Chakrabarti, C. L. Li, J. Zheng, P. J. Wang, H. X. Yin, Y. Qiu, B. Meng, and S. L. Yuan, Phys. Chem. Chem. Phys. **22**, 7058 (2020).

[32] P. Pramanik, D. C. Joshi, M. Reehuis, A. Hoser, J.-U. Hoffmann, R. S. Manna, T. Sarkar, and S. Thota, J. Phys.: Condens. Matter **32**, 245801 (2020).

[33] S. Nayak, K. Dasari, D. C. Joshi, P. Pramanik, R. Palai, V. Sathe, R. N. Chauhan, N. Tiwari, and S. Thota, Phys. Status Solidi B **253**, 2270 (2016).

[34] R. L. Miliard, R. C. Peterson, and B. K. Hunter, Am. Mineral. **80**, 885 (1995).